A R C H I V E S O F M E T A L L U R G Y A N D M A T E R I A L S
Volume 53 2008 Issue 4

K. ISHIDA*

RECENT PROGRESS ON Co-BASE ALLOYS – PHASE DIAGRAMS AND APPLICATION

AKTUALNY POSTĘP W BADANIACH STOPÓW NA OSNOWIE KOBALTU. WYKRESY FAZOWE I ZASTOSOWANIE

This paper presents recent progress on the phase diagrams and design for Co-base alloys, focusing on magnetic recording media, ferromagnetic Co-Ni-Al-base shape memory alloys, half-metallic Heusler alloys and Co-base superalloys. The calculated miscibility gap between ferromagnetic and paramagnetic states in the Co-X(X: Cr, Mo, W) systems has been found to agree well with the experimental results, strongly implying that the magnetic induced phase separation is responsible for the compositional heterogeneity in Co-base magnetic recording media. New ferromagnetic Co-Ni-Al shape memory alloys have also been developed based on phase diagrams, where the introduction of γ(Al structure) to the β(*B*2) matrix was found to drastically improve the ductility. The phase stability of half-metal Heusler Co-Cr base alloys is discussed in relation to the order-disorder transition, Curie temperature and the spin polarization ratio. Finally, the possibility of potent strengthening of Co-base superalloys by precipitation of the γ'($L1_2$) phase is presented.

Keywords: magnetic recording media, ferromagnetic shape memory alloy, Heusler alloy, Co-base superalloy

Praca przedstawia przegląd aktualnych badań nad wykresami fazowymi i projektowaniem stopów na osnowie kobaltu z ukierunkowaniem na środki magnetycznego przekazu, ferromagnetyczne stopy Co-Ni-Al-osnowie z pamięcią kształtu, pół-metaliczne stopy typu Heusler'a i superstopy na osnowie kobaltu. Wykazano, że obliczone zakresy rozwarstwienia pomiędzy stanam i ferromagnetycznymi i paramagnetycznymi w układach Co-X (X = Cr, Mo, W) zgadzają się z wynikami doświadczalnymi, wyraźnie wskazując na to, że wzbudzone magnetycznie rozdzielenie fazowe jest odpowiedzialne za złożoną niejednorodność w stopach na osnowie kobaltu z ukierunkowaniem na środki magnetycznego przekazu. Nowe ferromagnetyczne stopy Co-Ni-Al. z pamięcią kształtu zostały opracowane w oparciu o wykresy fazowe, także w przypadkach kiedy wprowadzenie γ(Al. struktury) do β(B2) osnowy powodowało drastyczny wzrost plastyczności. Stabilność fazowa pół-metalicznych stopów Heusler'a na osnowie Co-Cr jest dyskutowana w aspekcie przejścia porządek-nieporządek, temperatury Curie i jeżeli chodzi o stosunek spinowej polaryzacji. W efekcie końcowym, przedstawiona jest możliwość potencjalnego umocnienia superstopów na osnowie kobaltu drogą wydzielania fazy γ '($L1_2$).

1. Introduction

Cobalt-base alloys are widely used in various applications such as magnetic materials, corrosion and heat-resistant alloys, wear-resistant alloys, prosthetic alloys in medical parts etc., where the phase diagrams play a key role in material development.

In this paper, our recent research activities with regard to phase diagrams and applications of Co-base alloys are presented, focusing on the following alloy systems.

(1) Experimental and thermodynamic calculations on phase diagrams of Co-(Cr, Mo, W) base alloys for magnetic recording media.
(2) Phase diagram and microstructural evolution of Co-Ni-Al ferromagnetic shape memory alloy.
(3) Phase stability of half-metal-type Co-Cr base Heusler alloys.
(4) Co-base superalloys with γ + γ' structure.

2. Co-base magnetic recording media

Since the advent of Co-Cr alloy thin film as the first group of alloy materials to be used as "perpendicular magnetic recording" media,[1] it has been shown that Co-Cr-based film is made up of Co-rich ferromagnetic hexagonal-closed-packed (hcp) nanosized grains surrounded by a Co-poor paramagnetic hcp phase. This

* DEPARTMENT OF MATERIALS SCIENCE, GRADUATE SCHOOL OF ENGINEERING, TOHOKU UNIVERSITY, 6-6-02 AOBA-YAMA, SENDAI 980-8579, JAPAN

unique compositional modulation weakens the interparticle exchange interaction between the ferromagnetic grains, resulting in improvements of recording resolution as well as significant recording noise reduction.[2] Numerous investigations have been carried out to clarify the origin of the modulated microstructure and it has been suggested that the observed compositional inhomogeneity can be attributed to the "magnetically-induced miscibility gap" in the hcp phase[3]. This phase separation formed along the Curie temperature has been confirmed experimentally by the diffusion couple method[4]. Figure 1 shows the calculated phase diagram of the Co-Cr binary system, including the experimental data on the magnetically-induced miscibility gap and Gibbs energy-composition curve of the hcp phase at 400°C. Such a compositional modulation due to the magnetically induced phase separation in a hcp phase is easily developed during the thin-film growth process on heated substrates at around 500-700 K. It is well known that the addition of platinum and/or tantalum to Co-Cr-based high-density magnetic recording media modifies the recording characteristics, resulting in a drastic change in the distribution of chromium[5,6]. The thermodynamic calculation of the magnetically induced phase separation in the hcp phase of the Co-Cr-Pt and Co-Cr-Ta ternary systems has been conducted to explain the effect of the addition of platinum and tantalum on the chromium distribution in the Co-Cr-based alloys[7,8]. The calculated miscibility gap in the hcp phase of the Co-Cr-Pt system at 200°C is shown in Fig. 2(a). The miscibility gap is formed along the Curie temperature, and the width of the gap of the Co-Cr-binary becomes narrower with increasing platinum content. Kitakami et al. [9] have investigated the effect of platinum on the magnetic properties of Co-Cr thin films and concluded that the addition of platinum enhances the magnetic anisotropy energy (MAE) with a large coercivity because such addition reduces the chromium content in the cobalt-rich ferromagnetic phase. The calculated results reveal that the chromium content in the ferromagnetic hcp phase decreases with increasing platinum content, as shown in Fig. 2(a), which agrees well with the experimental data[5,10]. The isothermal section of the Co-Cr-Ta system at 400°C is shown in Fig. 2(b). The two-phase region is extended with increasing tantalum content and the chromium segregation is enhanced, whereas the chromium content in the ferromagnetic phase is not drastically reduced. This tendency qualitatively agrees with the results of the experimental data of Co-Cr-based thin films[5,11].

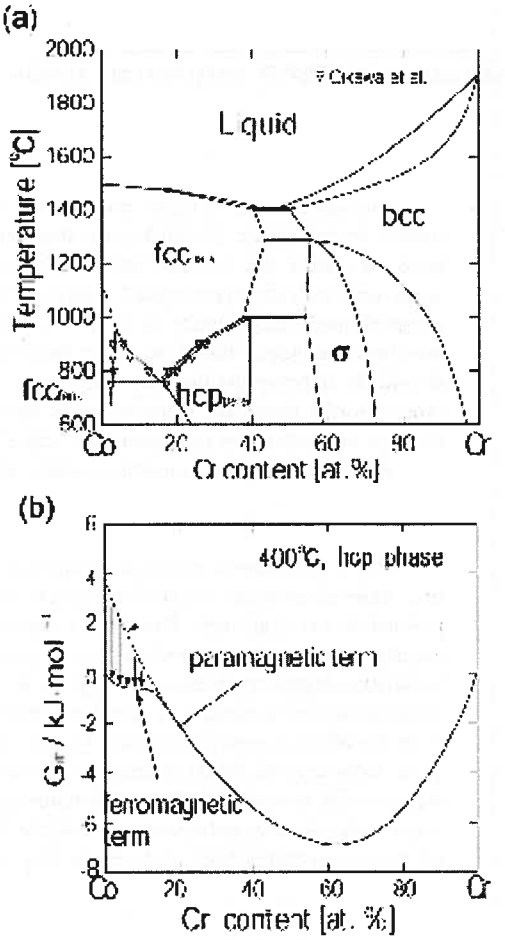

Fig. 1. (a) Calculated phase diagram of the Co-Cr binary system and (b) Gibbs energy-composition curve of hcp phase at 400°C

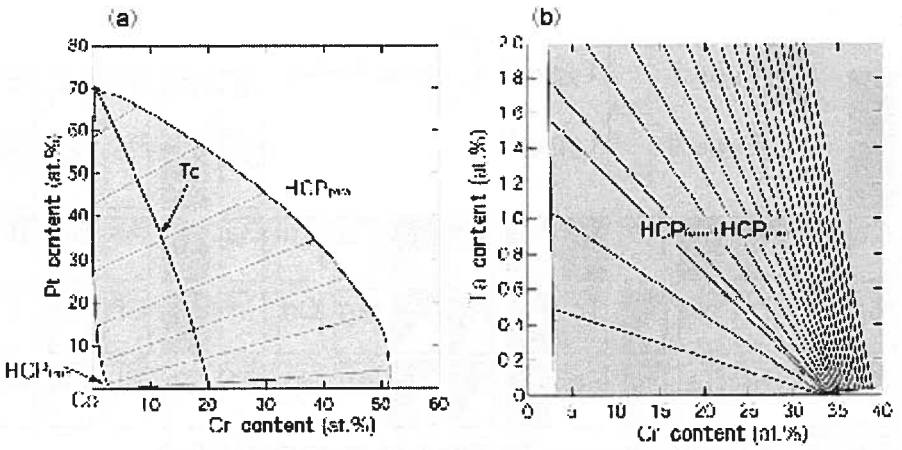

Fig. 2. Phase equilibria of (a) a Co-Cr-Pt system at 200°C and (b) a Co-Cr-Ta system at 400°C

From the thermodynamic calculation of the Co-Cr-X ternary system, the shape of the magnetically induced phase separation in the cobalt-rich portion can be classified into four types, as shown in Fig. 3[12]. In Type I, the chromium contents in both the ferromagnetic and paramagnetic phases decrease with an increasing amount of X. In Type II, the chromium content decreases in the ferromagnetic phase and increases in the paramagnetic phase with an increasing amount of X. In Type III, the chromium content of the paramagnetic phase is increased by the addition of X, whereas that in the ferromagnetic phase is not effectively reduced. Finally, in Type IV, the three-phase equilibrium of one ferromagnetic and two paramagnetic phases is formed. Figure 4 shows the classification of the effect of the alloying elements on the phase equilibria of the Co-Cr system in the periodic table based on the calculated results. Pd, Rh, and Ir show a type of miscibility gap similar to that of the Co-Cr-Pt phase diagram. The magnetic properties of the Co-Cr-Pd thin-film alloy would be expected to be similar to those of the Co-Cr-Pt system. On the other hand, the addition of iridium to cobalt strongly decreases the MAE, which in turn would cancel out the beneficial effect of decreasing chromium content in the ferromagnetic phase by the alloying of iridium[13]. This means that the MAE of each binary system, as well as the phase diagram, should be considered for the material design of Co-Cr-based high-density magnetic recording media.

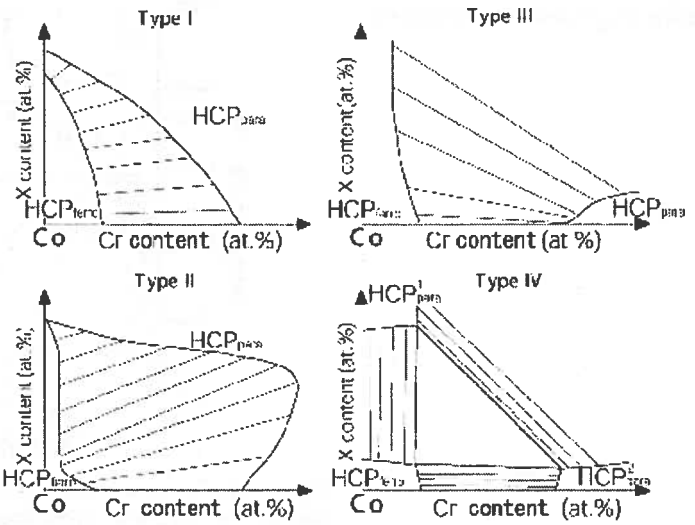

Fig. 3. Classification of phase separation in the hcp phase of the Co-Cr-X ternary system

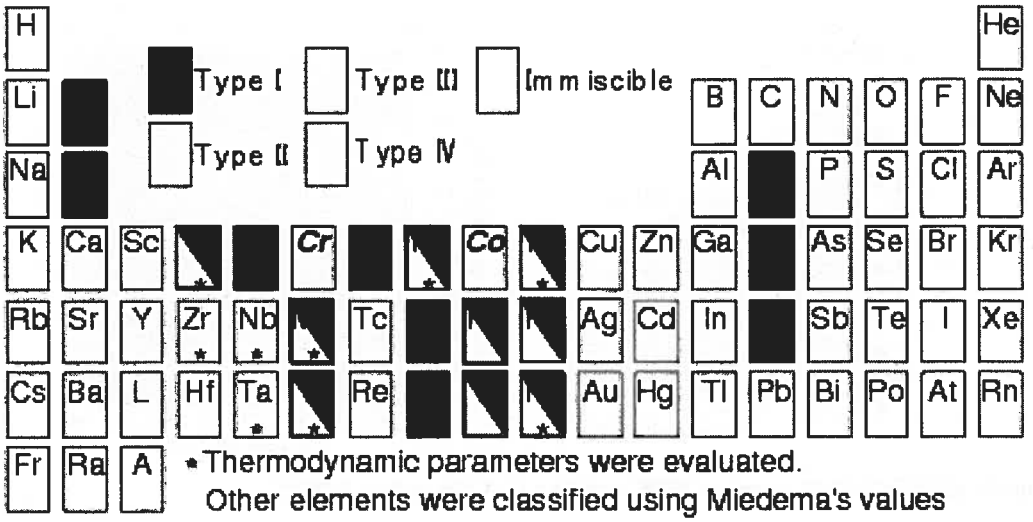

Fig. 4. Effect of alloying elements on the phase separation of the Co-Cr binary system

The magnetically-induced phase separation has also been confirmed in the Co-W binary system by the diffusion couple method. Figure 5 shows the calculated phase diagram of Co-W binary system compared with experimental data[14]. Based on the results, a nanoscale compositional fluctuation caused by magnetically induced phase separation has also been confirmed in films deposited on a heated substrate in analogy with Co-Cr based alloys as shown in Fig.6[15]. Figure 7 shows the in-plane magnetization curves of the films measured along NaCl [110] direction. The relatively large value of Hc for the film is associated with a large value of magnetocrystalline anisotropy materials. Consequently, the Co-W sputtered films as well as the Co-Mo films[16,17] are promising as next generation high-density magnetic recording media.

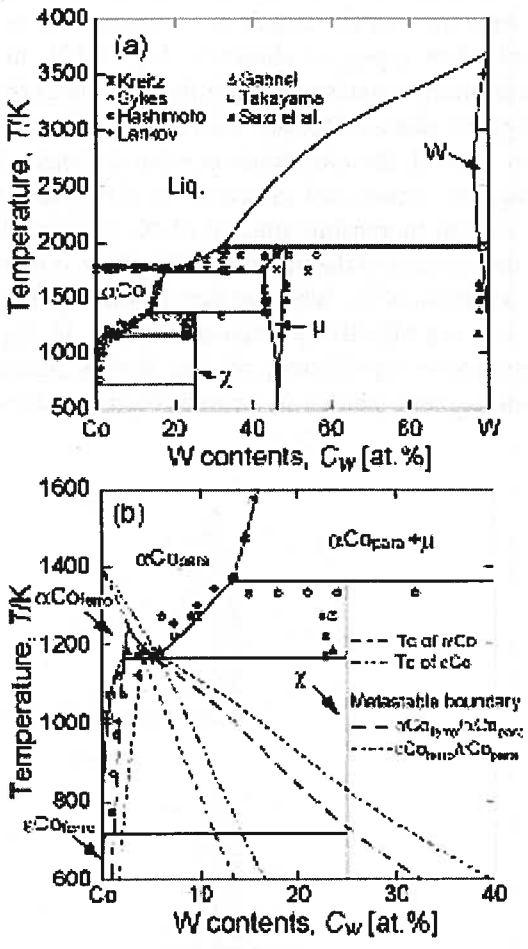

Fig. 5. Calculated phase diagram of the Co-W system: (a) whole system, (b) Co-rich corner, including the metastable phase boundaries

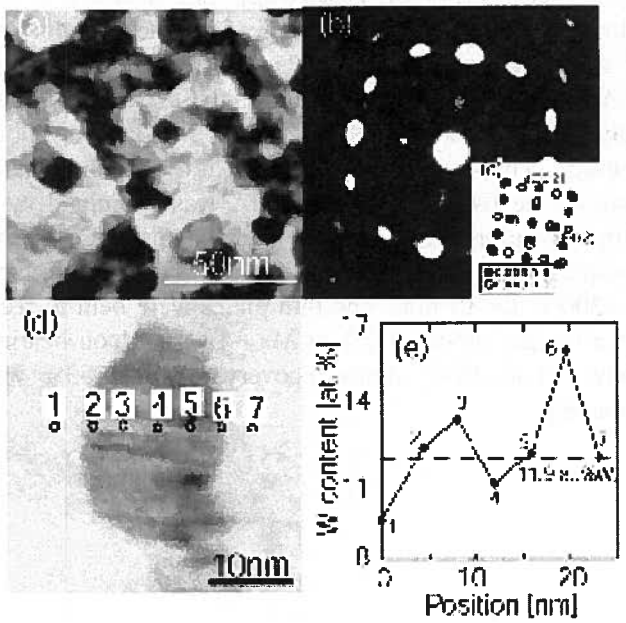

Fig. 6. Several kinds of data for Co-11.9 at% W – film deposited at 573 K

(a) TEM bright-field image,

(b) corresponding SAD pattern,

(c) indexed-electron-diffraction pattern,

(d) STEM bright-field image, and

(e) local composition at the numbered positions

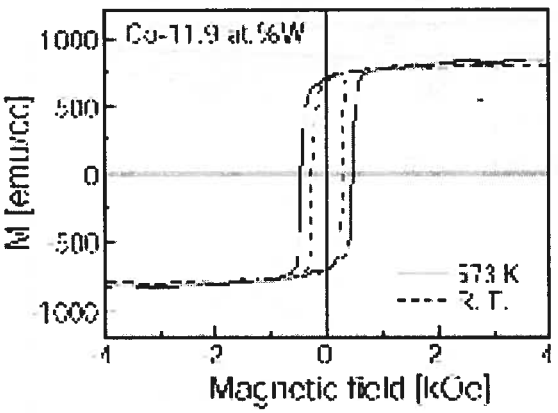

Fig. 7. Magnetization curves of Co-11.9 at% W films deposited at room temperature and at 573 K

3. Co-Ni-Al ferromagnetic shape memory alloys

Ferromagnetic shape-memory alloys (FSMAs) have received much attention as high-performance magnetically controlled actuator materials because they show a large magnetically induced strain by the rearrangement of twin variants in the martensite[18]. Several FSMA candidates have been reported, including Ni_2MnGa[18], Fe-Pd[19], and Fe_3Pt[20] alloys. Recently, the author's group has found a new group of FSMAs in Co-Ni-Al β (*B*2 structure)-based alloys[21–23].

In Fig. 8, the Curie temperature (*T*c), the martensitic transformation starting temperature (*M*s), and the reverse-transformation finishing temperature (Af) are plotted as a function of the Co content in the 30 at.% aluminum section[21]. The alloys show thermoelastic martensitic transformation from the β to the β' phase ($L1_0$ structure) accompanied by the shape-memory effect. *M*s increases and *T*c decreases with increasing Ni content. The phase transformation behavior of the alloys on cooling can be grouped into three types based on the characteristic features of the magnetic and martensitic transformations. In Type I, the paramagnetic β phase is magnetically transformed into the ferromagnetic β phase, and then martensitically transformed into the ferromagnetic β' phase (i.e., $T_C^{\beta} > Ms$). In Type II, the paramagnetic β' phase is directly transformed into the ferromagnetic martensite β' phase (i.e., $T_c^{\beta} < Ms < T_C^{\beta'}$). In Type III, the paramagnetic β phase is martensitically transformed into the paramagnetic β' phase and eventually ferromagnetic transition occurs in the β' phase (i.e., $T_C^{\beta} < Ms$). In the case of Type I alloys, the magnetization drastically increases and decreases at *A*s and *M*s temperatures[22], respectively. A large magnetocrystalline anisotropy energy of $Ku=3.9*10^6$ erg/cm^3 was confirmed in the martensite phase of the Co-Ni-Al β single crystal[23], being the same order of that of Ni_2MnGa. In the case of Type II alloys, the magnetization drastically decreases and increases at As and Ms temperatures, respectively. This is due to the difference in the Curie temperature between the β and β' phases.

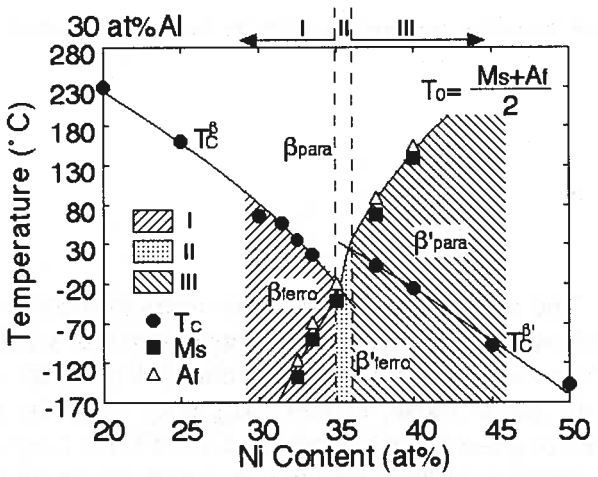

Fig. 8. Compositional dependence of the Curie temperature (Tc), the martensitic transformation temperature (Ms), and the austenite finishing temperature (Af) in $Co_xNi_{70-x}Al_{30}$ alloys

The presence of the fcc-γ solid solution as a second phase in the NiAl-β- based alloy system rendered the alloy ductile[24] and developed β + γ two-phase shape-memory alloys in the NiAl-β-based system, including Fe, Co and Mn[25–27]. The contours of iso-*M*s and iso-*T*c lines drawn on the basis of the experimental data are shown in Fig. 9 together with the phase boundaries of β+γ at 1100°C and 1300°C of the Co-Ni-Al ternary system[22,27]. The composition range of the β-phase alloy exhibiting the FSME is located near the β+γ two-phase boundary. β+γ two-phase FSMAs can be produced by a suitable choice of alloy composition and annealing temperature. The $Co_{40}Ni_{33}Al_{27}$ alloy was investigated as a typical β+γ two-phase FSMA[22]. The ductility of the alloy can be significantly improved by the introduction of a γ phase of about 7 vol%, as reported for other NiAl-β-based alloys[24–27], although the β single–phase polycrystalline alloys, as well as Ni_2MnGa show poor ductility. The shape-memory effect in the ferromagnetic state of the β+γ two-phase FSMA was examined by a simple bending test. A 150-μm thick specimen of the two-phase alloy was annealed at 1350°C for 2 min. and at 1300°C for 15 min. The thin plates were bent to realize a surface strain of 2% at Ms (-13°C). Upon heating above Af to 26°C, shape recovery of about 83% was obtained.

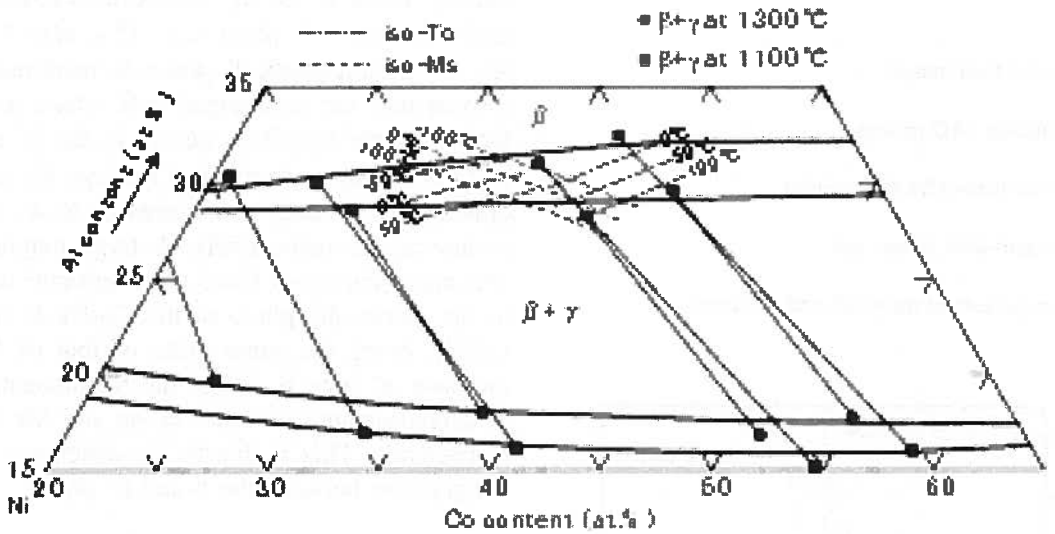

Fig. 9. Tc and Ms temperatures related to the phase diagram of the Co-Ni-Al ternary system

The superelastic and shape recovery properties depend on the grain size[28], the large grain size yielding to improve these properties. To obtain a large grain size of the parent phase, $Co_{40}Ni_{32}Al_{28}$ alloy including a γ phase of about 8% was annealed at 1350°C for 1 day and at 1260°C for 1 hour, resulting in growth of the average grain size of the β phase to about 3 mm. Figure 10 shows the tensile stress-strain curve of this sample with *M*s=-13 and Af=-10°C at (Af+12) °C. Complete superelasticity cannot be obtained in the first cycle; however, complete SE can be obtained from the second cycle. In addition, the critical transition stress σ_t and stress hysteresis (indicated by the vertical arrows) obviously decrease from the first cycle to the second cycle. These SE behaviors are in accord with the SE behaviors obtained from the β+γ two-phase alloy in compression and would be caused by the residual stress induced around the γ phase[29]. Consequently, a maximum value of tensile SE strain of about 6.3% was obtained in this large β grain sample.

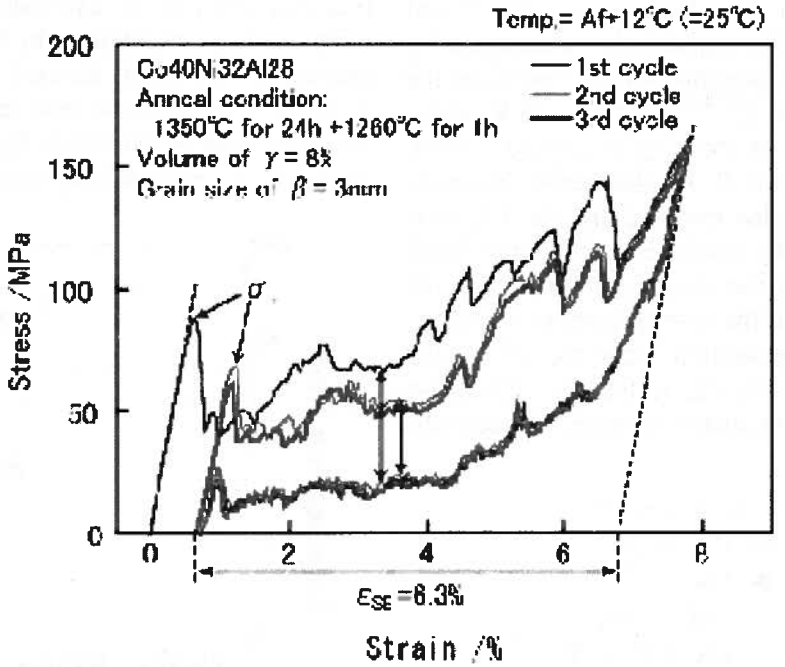

Fig. 10. Tensile cyclic stress-strain curves in $Co_{40}Ni_{32}Al_{28}$ alloy with a large average β grain size of about 3 mm

4. Phase stability and half-metallic properties of Co-Cr-base heusler alloys

Half-metallic ferromagnets (HMFs) are currently of great interest in the field of spintronics in order to realize spin-dependent devices with high performance, and many $L2_1$ (full-Heusler)-type HMFs have been extensively studied from both theoretical and experimental viewpoints. Recent band calculations have shown clear evidence for the HMFs from the electronic structures of $L2_1$ and $B2$-type Co_2CrAl alloys[30,31,32]. However, experimental values of the saturation magnetic moment, Ms, and the spin polarization of the $L2_1$ and $B2$-type Co_2CrAl alloys are much lower than the theoretical values[33,34]. Recently, we have demonstrated that an inevitable $A2$ + $B2$ spinodal decomposition which appears in the Cr-rich portion of $Co_2Cr_{1-x}Fe_xAl$ alloys significantly reduces the half-metallic magnetic properties. Since half-metallic properties including spin polarization strongly depend on the crystal structure and the degree of order, detailed information on the phase stability is useful for realizing HMF characteristics[35,36].

The phase stability of Co-Cr-Ga and Co-Cr-Fe-Ga Heusler alloys have been investigated[37–40] Figure 11 shows the vertical section diagram of 50 at%Co in the Co-Cr-Ga ternary system. The T_c and $T_t^{B2/L21}$ temperatures increase with the Ga content, and the maxima of T_c and $T_t^{B2/L21}$ converge with the stoichiometric content of Co_2CrGa. It is also shown that the measured $T_t^{B2/L21}$ curve is in good agreement with the Bragg-Williams-Gorsky (BWG) approximation, where the calculated $T_t^{B2/L21}$ is described by a parabolic curve as a function of atomic content, and the maximum $T_t^{B2/L21}$ is at the stoichiometric (Co_2CrGa) composition. Consequently, the $L2_1$-type single-phase alloys in the Co-Cr-Ga system can be easily obtained by quenching, in contrast to the Co-Cr-Al alloy system which exhibits an inevitable $A2$ +$B2$ spinodal decomposition.

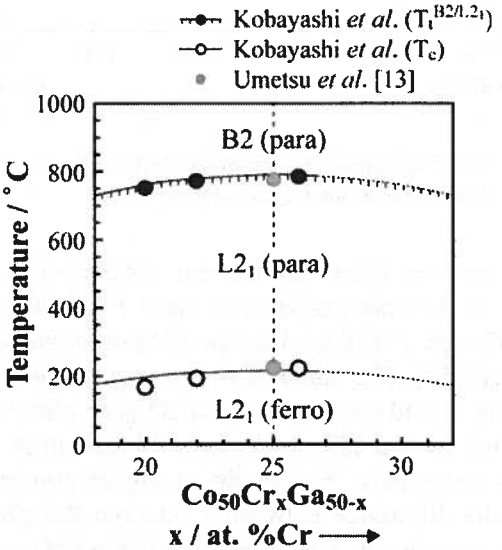

Fig. 11. Vertical section diagram of 50 at% Co in the Co-Cr-Ga ternary system

Figure 12 shows a metastable phase diagram of the $Co_2Cr_{1-x}Fe_xGa$ alloy system,[36] together with data on the $Co_2Cr_{1-x}Fe_xAl$ alloy system[35]. The bold hatched and dotted lines represent the transition tem-

perature from the $L2_1$ to the B2-type phase $T_t^{B2/L21}$ and the Curie temperature T_c, respectively, determined by DSC measurements. The transition temperature from the $L2_1$ to the $B2$-type phase $T_t^{B2/L21}$ is 1082 ±13 K, about 150 K higher than that of the $Co_2Cr_{1-x}Fe_xAl$ system, and the Curie temperature T_c monotonically increases with increasing x. It is also revealed that the $L2_1$-type single-phase can be easily obtained in the entire range of x for the $Co_2Cr_{1-x}Fe_xGa$ system, in contrast to the $Co_2Cr_{1-x}Fe_xAl$ system in the Cr-rich portion which exhibits a spinodal decomposition from the $B2$ to the $A2 + B2$ phase and from the $L2_1$ to the $A2 + L2_1$ phase in the higher and lower temperature range, respectively.

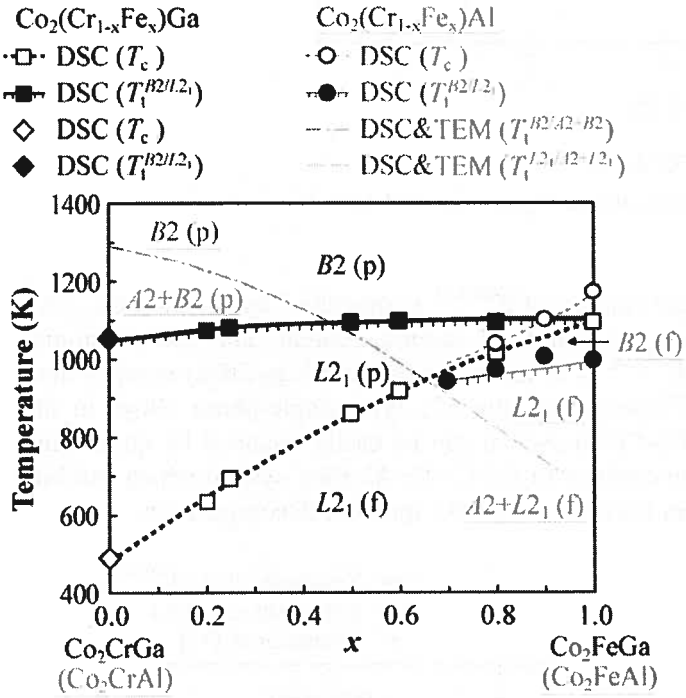

Fig. 12. Metastable phase diagram of the $Co_2Cr_{1-x}Fe_xGa$ alloy system compared with that of the $Co_2Cr_{1-x}Fe_xAl$ system

Based on these results, the concentration dependence of the spin polarization ratio P (%) for the $L2_1$ and $B2$-type $Co_2(Cr_{1-x}Fe_x)Ga$ alloy systems is shown in Fig.13[38]. The value of P becomes smaller with increasing x, and the value of the $B2$-type phase is lower than that of the $L2_1$-type phase in the entire concentration range of x. Especially, at higher concentrations of x, the difference between P in both the phases becomes significant. For x = 1.00 (≡Co_2FeGa), the ratio of P for the $L2_1$-type phase is 37%, resulting in a remarkable reduction of the half-metallic property. For practical applications, half-metallic ferromagnets having a high spin polarization ratio P with a high Curie temperature T_c are highly desired. Accordingly, high values of the spin polarization ratio and the Curie temperature are obtainable by adjusting the amount of Fe for Cr in the $Co_2(Cr_{1-x}Fe_x)Ga$ alloy system.

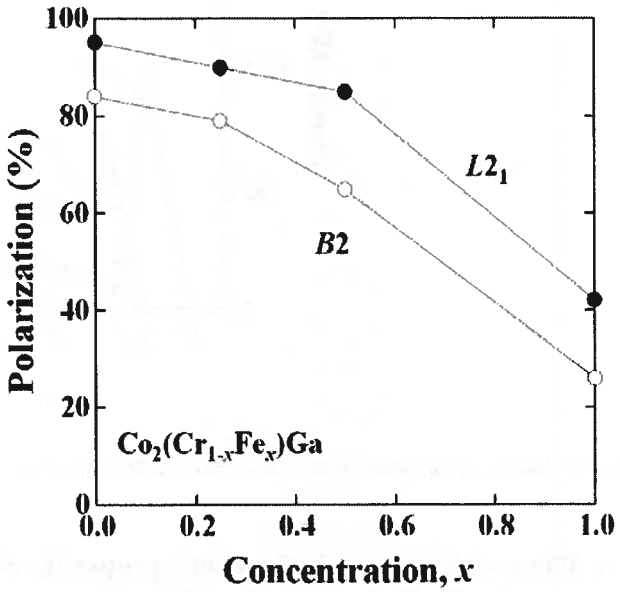

Fig. 13. Concentration dependence of the spin polarization ratio of the $L2_1$ and $B2$-type phases of the $Co_2(Cr_{1-x}Fe_x)Ga$ alloy system

Bcc metastable phase diagrams of the $Co2Cr(Ga_{1-y}Al_y)$, $Co_2Fe(Ga_{1-y}Al_y)$ and $Co_2(Cr_{1-x}Fe_x)Al$ alloy systems are shown in Fig. 14[37,40]. The bold hatched and dotted lines represent the $T_t^{B2/L21}$ and T_c, respectively, determined by DSC measurements and TEM observations. In the case of the $Co_2Cr(Ga_{1-y}Al_y)$ section shown in Fig. 14(a), while the T_c is almost constant at about 480 K, the $T_t^{B2/L21}$ linearly decreases with increasing y from about 1050 K. Although the $A2 + B2$ two-phase region appears in the Al-rich side, the $T_t^{B2/L21}$ and the T_c of the metastable Co_2CrAl alloy can be estimated as being 800 and 470 K, respectively, by extrapolation from the Ga-rich side. These values are in good agreement with the those extrapolated from the $Co_2(Cr_{1-x}Fe_x)Al$ section as shown in Fig. 14(b). On the other hand, the T_c is always located at temperatures above the $T_t^{B2/L21}$ and there is no $A2 + B2$ two-phase region in the $Co_2Fe(Ga_{1-y}Al_y)$ section as shown in Fig. 14(c). In this system, while the $T_t^{B2/L21}$ decreases with increasing y, as does that in the $Co_2Cr(Ga_{1-y}Al_y)$ system, the T_c slightly increases from about 1100 K to about 1170 K.

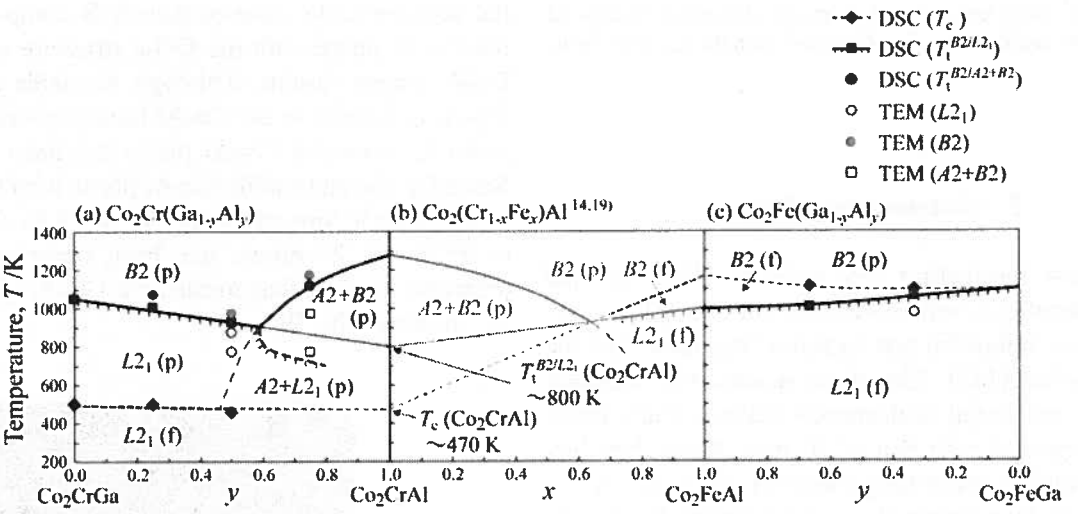

Fig. 14. Metastable phase diagrams of the bcc phase in the $Co_2Cr(Ga_{1-y}Al_y)$ and $Co_2Fe(Ga_{1-y}Al_y)$ alloy systems together with data on the $Co_2(Cr_{1-x}Fe_x)Al$ system. The bold hatched and dotted lines represent the transition temperature $T_C^{B2}/L2_1$ from the $B2$ to $L2_1$-type phase and the Curie temperature Tc, respectively, determined by DSC measurement and TEM observation

The polarization P of the $L2_1$ and $B2$-type phases has been theoretically evaluated in the $Co_2(Cr_{1-x}Fe_x)Al$ and $Co_2(Cr_{1-x}Fe_x)Ga$ sections[38,41], which shows that the $L2_1$ Heusler phase in the Cr-rich region of both the sections has a high value of polarization. Figure 15 shows the iso-polarization lines in the $Co_2(Cr_{1-x}Fe_x)(Ga_{1-y}Al_y)$ alloy system[40]. If it is assumed that the polarization P of $Co_2(Cr_{1-x}Fe_x)(Ga_{1-y}Al_y)$ alloys can be expressed by linear interpolation from the $Co_2(Cr_{1-x}Fe_x)Al$ and $Co_2(Cr_{1-x}Fe_x)Ga$ sections, the gray area in Fig. 15 is expected to be a suitable concentration area for obtaining excellent half-metallic properties ($P \geqq 80\%$), high Tc ($\geqq$ 573 K), and high stability of $L2_1$-type single-phase ($T_t^{B2/L21} \geqq 973$ K).

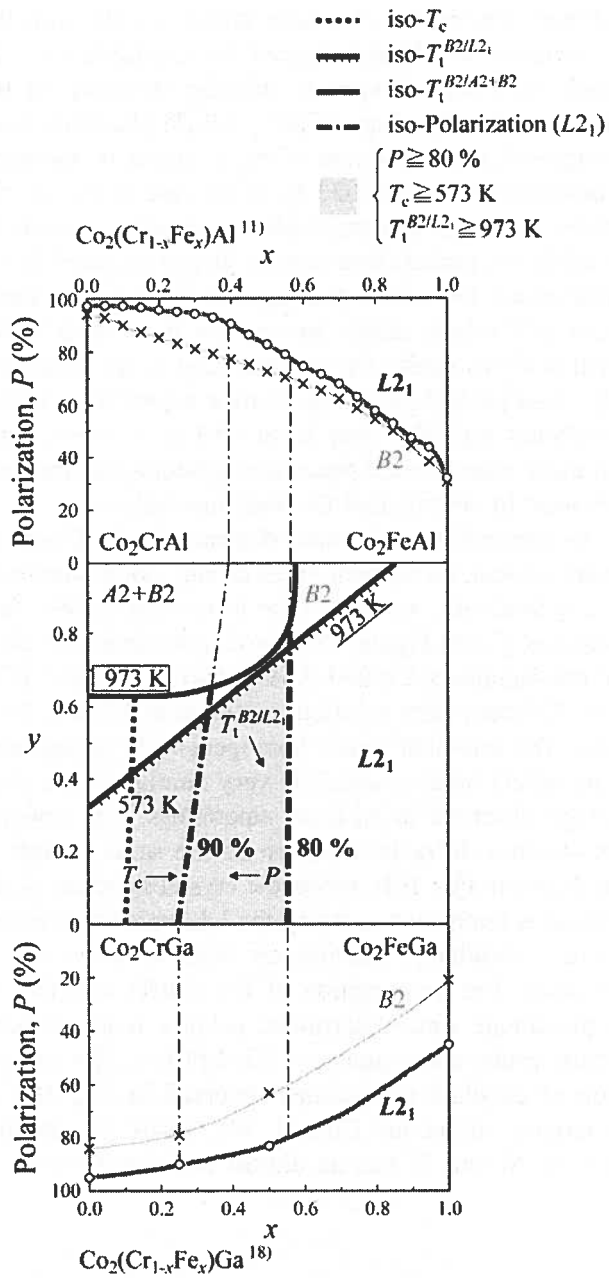

Fig. 15. Iso-polarization lines in the $Co_2(Cr_{1-xFex})(Ga_{1-y}Al_y)$ al-

loy system by linear interpolation from the theoretical results for $Co_2(Cr_{1-x}Fe_x)Al$ and $Co_2(Cr_{1-x}Fe_x)Ga$ alloys with the $L2_1$-type structure

5. Co-base superalloys

The most fascinating heat-resistant alloys are the Ni-base superalloys, which are used, for example, in aircraft engines, industrial gas turbines, reactors, and the chemical industry[42]. The main reason why Co-base alloys have not found widespread usage is their lower strength compared with that of Ni-base alloys, but they have been studied for a long time[43]. With the development of Ni-base superalloys strengthened by the ordered γ' $Ni_3(Al, Ti)$ phase, the possibilities of precipitation hardening using geometrically close-packed phases that have the form of A_3B have been extensively investigated. Two types of geometrically close-packed phases have been reported in Co-base alloys: Co_3Ti with the $L1_2$ structure[44,45] and ordered fcc Co_3Ta[46,47]. Although the effect of various alloying elements on the stability and morphology of the γ' Co_3Ti phase has been investigated, the usefulness of the γ' phase is restricted to temperatures below 1023 K. In the case of Co_3Ta, the ordered fcc phase is metastable and readily converts to the stable hexagonal close-packed (hcp) structure Co_3Ta. Furthermore, the lattice parameter mismatches of these phases in Co-base alloys are usually more than 1.0%, which is not as useful for strengthening as the geometrically close-packed phases in Ni-base superalloys, where mismatches typically vary from –0.1 to + 0.5%. Geometrically close-packed phase strengthening has thus not been used in commercial Co-base superalloys.

In determining the phase diagram of the Co-Al-W ternary system, we found a stable ternary compound with the $L1_2$ structure, which has the form $Co_3(Al, W)$, designated as γ'.[48] Figure 16A shows a transmission electron micrograph of Co-9Al-7.5W (at%) annealed at 1173 K for 72 hours after solution treatment at 1573 K for 2 hours. The cuboidal phase homogeneously precipitates in the γ(A1) matrix, which is very similar to the morphology observed in Ni-base superalloys. The selected area electron diffraction pattern of the same sample is also shown in Fig. 16B, where the crystal structure of the γ' phase is confirmed as being the $L1_2$ ordered structure and the cuboidal γ' precipitates align in the < 001 > directions. The composition of the matrix and that of the precipitate were determined using a field emission electron probe micro-analyzer (FE-EPMA). The composition of cuboidal precipitates observed in Fig. 16A is the ternary compound $Co_3(Al, W)$, where the composition of Al and W has an almost equiatomic ratio. In the geometrically close-packed A_3B compound, the stable Co_3W phase with the DO_{19} structure appears in the Co-W binary system. Although no stable compound of Co_3Al is formed in the Co-Al binary system, the formation of an ordered Co_3Al phase has been reported[49]. Recently, the metastable Co_3Al phase with the $L1_2$ structure, which is formed in the Co-14at%Al alloy annealed at 873K for 24 hours, has been observed[50]. It can therefore be said that metastable Co_3Al γ' is stabilized by alloying with W.

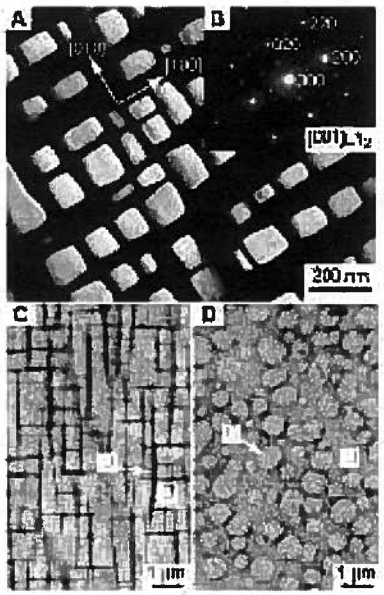

Fig. 16. Election micrographs of Co- 9Al-7.5W alloy annealed at 1173 K for 72 hours. (A) Dark field image. (B) Selected area diffraction pattern. (C and D) Field emission scanning electron micrographs of Co-8.8Al-9.8W-2Ta (C) and Co-8.8Al-9.8W- 2Mo (D) annealed at 1273 K for 1 week

Figures 17A and B, show isothermal section diagrams determined experimentally in the present study, as well as recent data on the Co-W binary system at 1173 and 1273 K, respectively. The γ' phase is stable at 1173 K but metastable at 1273 K. The thermal stability of the γ' phase and the effect of alloying were investigated by differential scanning calorimetry (DSC). Figure 18A shows the DSC curves on heating, where the solvus temperature was determined from the endothermic peak, as indicated by arrows. The DSC curve of Waspaloy [Ni-21Cr-2.5Mo-13Co-2.9Al-3.5Ti-0.3C (at%)], a widely used commercial Ni-base superalloy, is also shown. The solvus temperatures of the γ' phase in the Co-Al-W ternary system is ~1263 K, which corresponds well with the phase diagram, as shown in Fig.17. The addition of Ta stabilizes the γ' phase such that the solvus temperature is ~1373 K, a value higher than that of Waspaloy. The addition of Nb or Ti shows a similar effect. Recent work has also shown that the addition of Ni increas-

es the γ' solvus[51]. It can also be seen from Fig.18A that the melting temperatures of Co-Al-W-base alloys are ~1673 K, which is 50 to 100 K higher than those of Ni-base superalloys. Figure 18B shows the temperature variation of Vickers hardness of the γ+γ' structure for Co-9.2Al-9W and Co-8.8Al-9.8W-2Ta aged at 1073 K for 24 hours after solution treatment at 1573 K for 2 hours. Aging treatment of Waspaloy was carried out at 1118 K for 24 hours and 1033 K for 16 hours after solution treatment at 1353 K for 4 hours. The hardness of the γ+γ' structure of the Co-9.2Al-9W alloy is very similar to that of Waspaloy. The addition of Ta increases the hardness, which might be due to the stabilization of the γ' phase up to 1373K. Figure 19 shows the temperature dependence of 0.2% flow stress at high temperature in Co-base alloys compared with the conventional Ni-base superalloys[52–54]. It should be noted that the flow stress shows a strong positive dependence on temperature above 600°C and that the strength of Co-9Al-10W-2Ta is comparable to or higher than that of nickel-based superalloys above 900°C. The flow stress anomalies are attributed to the activation of multiple slip modes within the γ' phase, which include the slip of < 110 > dislocations below the peak and the thermally activated slip of < 112 > dislocations above the peak[52]. Finally, we also identified a ternary compound, γ' $Ir_3(Al,W)$, with the $L1_2$ structure[48], which suggests that the Co-Ir-Al-W-base systems with γ+γ' $(Co,Ir)_3$ (Al,W) structures offer great promise as candidates for next-generation high-temperature materials.

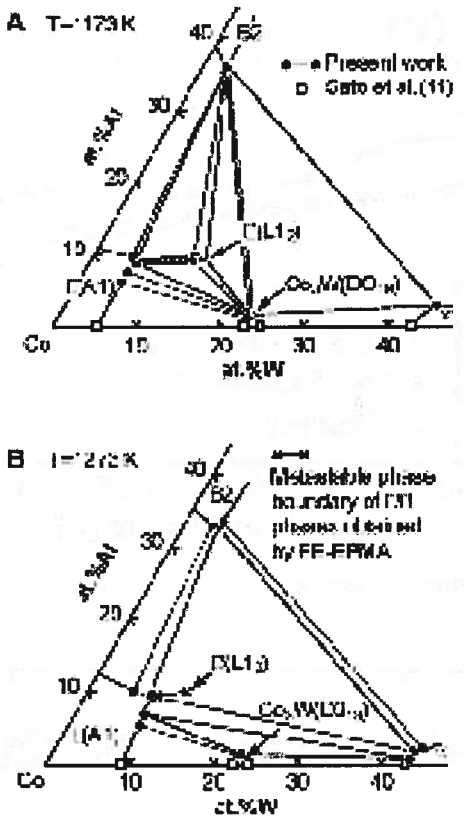

Fig. 17. Isothermal section diagrams of the Co-Al-W ternary system in the Co-rich portion at (A) 1173 K and (B) 1273 K

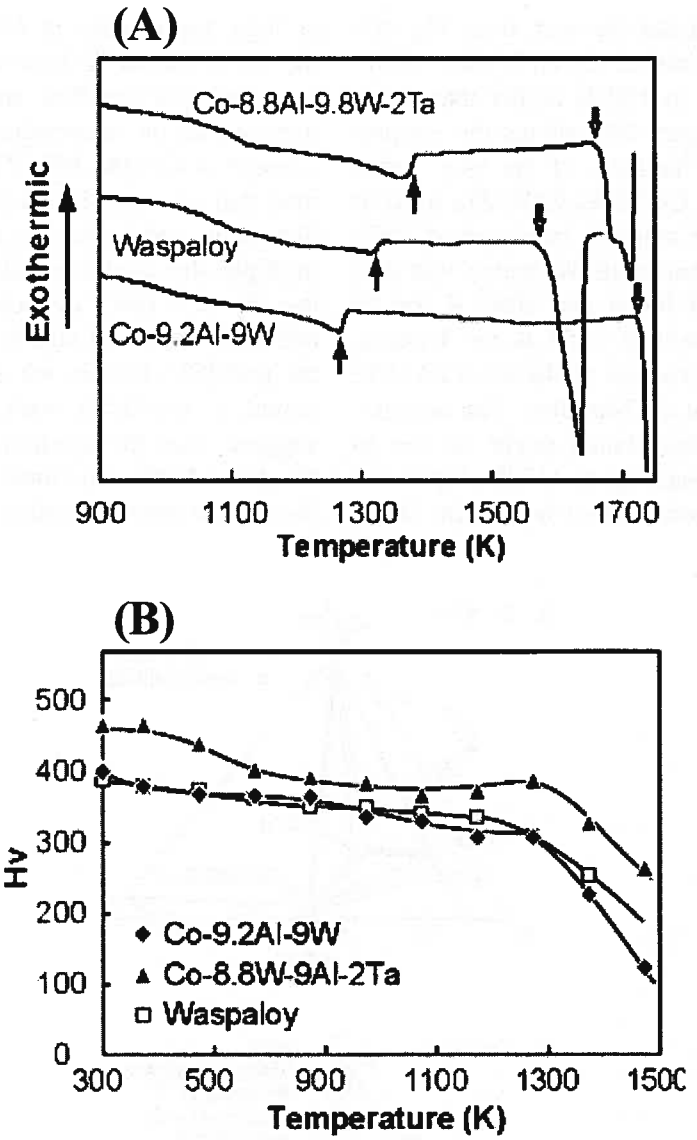

Fig. 18. (A) DSC curves and (B) High-temperature Vickers hardness

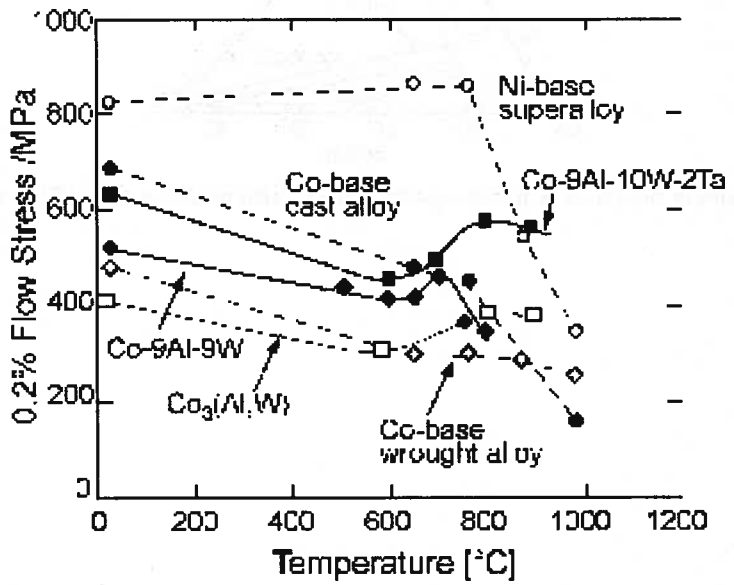

Fig. 19. Temperature dependence of 0.2% flow stress at high temperature of Co-based alloys

6. Summary

The phase diagrams and the related microstructural control of Co-base alloys were presented focusing on magnetic recording media, ferromagnetic shape memory, and half-metallic ferromagnets and heat-resistant superalloys. The magnetically- induced miscibility gap is the origin of the compositional modulation of Co-Cr base magnetic recording media. A similar phase separation was confirmed in the Co-W and Co-Mo thin films. New ductile ferromagnetic Co-Ni-Al shape memory alloys have been developed, the introduction of γ (Al) phase to the β ($B2$) matrix resulting in drastic improvement of ductility. The β+γ Co-Ni-Al alloy with large grain size shows about 6% tensile superelasticity. The phase stability of half-metal Heusler Co-Cr base alloys, particularly the order-disorder phase transition from $L2_1$ to $B2$ phase is strongly related to the spin polarization ratio. Finally, a newtype of Co-base superalloys strengthened by the precipitation of the Co_3 (Al, W) phase with the $L1_2$ structure in the γ matrix was shown. The Co-base superalloys show the positive temperature dependence of flow stress above 600°C and their strength is comparable or higher to that of Ni-base conventional superalloys.

Acknowledgements

The author would like for thank Profs. R. Kainuma, K. Oikawa, I. Ohnuma, S. Sutou, Drs. T. Omori, R. Umetsu, S. Kobayashi, H. Morito, Y. Tanaka for their help in preparing the manuscript. This work was supported by a Grant-in-Aid for Scientific Research from the Ministry of Education, Science, Sports and Culture, Japan and Core Research for Evolutional Science and Technology (CREST), Japan Science and Technology Agency (JST).

REFERENCES

[1] S. Iwasaki, Y. Nakamura, IEEE Trans. Magn. Mag. **13**, 1272-1277 (1997).
[2] Y. Maeda, M. Takahashi, Jpn. J. Appl. Phys. **28**, L248-L251 (1989).
[3] K. Ishida, T. Nishizawa, User Aspects of Phase Diagrams, F. H. Hayes, ed., The Institute of Metals, 185-198 (1991).
[4] K. Oikawa, G. W. Qin, T. Ikeshoji, R. Kainuma, K. Ishida, Acta. Mater. **50**, 2223-2232 (2002).
[5] N. Inaba, T. Yamamoto, Y. Hosoe, M. Futamoto, J. Magn. Magn. Mater. **168**, 222-231 (1997).
[6] Y. Hirayama, M. Futamoto, K. Kimoto, K. Usami, IEEE Trans. Magn. Mag., MAG-32, 3807-3809 (1996).
[7] K. Oikawa, G. W. Qin, T. Ikeshoji, O. Kitakami, Y. Shimada, K. Ishida, K. Fukamichi, J. Magn. Magn. Mater. **236**, 220-233 (2001).
[8] K. Oikawa, G. W. Qin, O. Kitakami, H. Shimada, K. Ishida, K. Fukamichi, J. Magn. Soc. Jpn. **25**, 478-485 (2001).
[9] O. Kitakami, O. Kitakami, N. Kikuchi, S. Okamoto, Y. Shimada, K. Oikawa, Y. Otani, K. Fukamichi, J. Magn. Magn. Mater. **202**, 305-310 (1999).
[10] K. Hono, S. S. Babu, Y. Maeda, N. Hasegawa, T. Sakurai, Appl. Phys. Lett. **62**, 2504-2506 (1993).
[11] R. D. Fisher, J. C. Allan, J. L. Pressesky, IEEE Trans. Magn. **22**, 352-354 (1986).
[12] K. Oikawa, G. W. Qin, O. Kitakami, Y. Shimada, K. Fukamichi, K. Ishida, Appl. Phys. Lett. **79**, 644-646 (2001).
[13] N. Kikuchi, O. Kitakami, S. Okamoto, Y. Shimada, A. Sakuma, Y. Otani, K. Fukamichi, J. Phys. Condens. Mater. **11**, L485-L490 (1999).
[14] J. Sato, K. Oikawa, R. Kainuma, K. Ishida, Mater Trans. **46**, 1199-1207 (2005).
[15] K. Oikawa, G. W. Qin, M. Sato, S. Okamoto, O. Kitakami, Y. Shimada, K. Fukamichi, K. Ishida, T. Koyama, Appl. Phys. Lett. **85**, 2559-2561 (2004).
[16] K. Oikawa, F. W. Qin, M. Sato, O. Kitakami, Y. Shimada, J. Sato, K. Fukamichi, K. Ishida, Appl. Phys. Lett. **83**, 966-968 (2003).
[17] G. W. Qin, K. Oikawa, M. Sato, O. Kitakami, Y. Shimada, K. Fukamichi, K. Ishida, IEEE Trans. Mag. **41**, 918-920 (2005).
[18] K. Ullakko, J. K. Huang, C. Kantner, R. C. O'Handley, V. V. Kokorin, Appl. Phys. Lett. **69**, 1996-1998 (1996).
[19] R. D. James, M. Wuttig, Philos. Mag. **A77**, 1273-1299 (1998).
[20] T. Kakeshita, T. Takeuchi, T. Fukuda, T. Saburi, R. Oshima, S. Muto, K. Kishio, Mater. Trans. JIM, **41**, 882-887 (2000).
[21] K. Oikawa, T. Ota, F. Gejima, T. Omori, R. Kainuma, K. Ishida, Mater. Trans. **42**, 2472-2475 (2001).
[22] K. Oikawa, L. Wulff, T. Iijima, F. Gejima, T. Omori, A. Fujita, K. Fukamichi, R. Kainuma, K. Ishida, Appl. Phys. Lett. **79**, 3290-3292 (2001).
[23] H. Morito, A. Fujita, K. Fukamichi, K. Oikawa, R. Kainuma, K. Ishida, Appl. Phys. Lett. **81**, 1657-1659 (2002).
[24] K. Ishida, R. Kainuma, N. Ueno, T. Nishizawa, Metall. Trans. **22A**, 441-446 (1991).
[25] R. Kainuma, K. Ishida, T. Nishizawa, Metall. Trans. **23A**, 1147-1153 (1992).
[26] R. Kainuma, H. Nakano, K. Oikawa, K. Ishida, T. Nishizawa, Mater. Res. Soc. Proc. **246**, 403-408 (1992).

[27] R. Kainuma, M. Ise, C. C. Jia, H. Ohtani, K. Ishida, Intermetallics **4**, S151-S158 (1996).
[28] Y. Tanaka, K. Oikawa, Y. Sutou, T. Omori, R. Kinuma, K. Ishida, Materials Science and Engineering A **438-440**, 1054-1060 (2006).
[29] C. Efstathiou, H. Sehitoglu, A. J. W. Johnson, R. F. Hamilton, H. J. Maier, Y. Chumlyakov, Scripta Mater. **51**, 979-985 (2004).
[30] H. J. Elmers, S. Wurmehl, G. H. Fecher, G. Jakob, C. Felser, G. Schönhense, Appl. Phys. A: Mater. Sci. Process. **79**, 557-563 (2004).
[31] S. Ishida, S. Kawakami, S. Asano, Mater. Trans. **45**, 1065-1069 (2004).
[32] Y. Miura, K. Nagao, M. Shirai, J. Appl. Phys. **95**, 7225-7227 (2004).
[33] K. Inomata, S. Okamura, N. Tezuka, J. Magn. Magn. Mater. **282**, 269-274 (2004).
[34] S. Okamura, R. Goto, N. Tezuka, S. Sugimoto, K. Inomata, J. J. Appl. Phys., Part 1 **28**, 172- (2004).
[35] K. Kobayashi, R. Y. Umetsu, R. Kainuma, K. Ishida, T. Oyamada, A. Fujita, K. Fukamichi, Appl. Phys. Lett. **85**, 4684-4686 (2004).
[36] K. Kobayashi, R. Y. Umetsu, A. Fujita, K. Oikawa, R. Kainuma, K. Fukamichi, K. Ishida, J. Alloys Compd. **399**, 60-63 (2005).
[37] R. Y. Umetsu, K. Kobayashi, R. Kainuma, A. Fujita, K. Fukamichi, K. Ishida, A. Sakuma, Appl. Phys. Lett. **85**, 2011-2013 (2004).
[38] R. Y. Umetsu, K. Kobayashi, A. Fujita, K. Oikawa, R. Kainuma, K. Ishida, N. Endo, K. Fukamichi, A. Sakuma, Phys. Rev. **B72**, 214412-1-214412-7 (2005).
[39] K. Kobayashi, R. Kainuma, K. Fukamichi, K. Ishida, J. Alloys and Compounds **403**, 161-167 (2005).
[40] K. Kobayashi, R. Kainuma, K. Ishida, Mater. Trans. **47**, 20-24 (2006).
[41] Y. Miura, K. Nagao, M. Shirai, Phys. Rev. B **69**, 144413-1-144413-7 (2004).
[42] R. F. Decker, C. T. Sims, in The Superalloys, C. T. Sims, W. C. Hagel, Eds. (Willey, New York), 33-77 (1972).
[43] C. T. Sims, in The Superalloys, C. T. Sims, W. C. Hagel, Eds. (Wiley, New York), 145–174 (1972).
[44] J. M. Blaise, P. Viatour, J. M. Drapier, Cobalt 49, 192-195 (1970).
[45] P. Viatour, J. M. Drapier, D. Coutsouradis, Cobalt **3**, 67-74 (1973).
[46] J. M. Drapier, J. L. de Brouwer, D. Coutsouradis, Cobalt **27**, 59-72 (1965).
[47] J. M. Drapier, D. Coutsouradis, Cobalt **39**, 63-74 (1968).
[48] J. Sato, T. Omori, K. Oikawa, I. Ohnuma, R. Kainuma, K. Ishida, Science **312**, 90-91 (2006).
[49] A. J. Bradley, G. C. Seager, J. Inst. Met. **64**, 81-91 (1939).
[50] T. Omori, Y. Sutou, K. Oikawa, R. Kainuma, K. Ishida, Mater. Sci. Eng. A **438-440**, 1045-1049 (2006).
[51] K. Shinagawa, T. Omori, J. Sato, K. Oikawa, I. Ohnuma, R. Kainuma, K. Ishida, Mater. Trans. **49**, 1474-1479 (2008).
[52] A. Suzuki, G. C. Denolf, T. M. Pollock, Scri. Mater. **56**, 385-388 (2007).
[53] S. Miura, K. Ohkubo, T. Mohri, Mater. Trans. **48**, 2403-2408 (2007).
[54] A. Suzuki, T. M. Pollock, Acta Mater. **56**, 1288-1297 (2008).

Received: 10 September 2008.